SSC19-XII-03

Simulation of a High Stability Reference Clock for Small Satellites with Modeled GPS Timing Errors

Damon Van Buren
University of Colorado, Boulder, Space Signal Sciences LLC
12996 S. Carson Ct., Parker, CO 80134; (720) 504-2703
damon@spacesigsci.com

Scott Palo, Penina Axelrad
University of Colorado, Boulder
Colorado Center for Astrodynamics Research
431 UCB, Boulder, CO 80309; (303) 735-4900
Scott.Palo@colorado.edu, Penina.Axelrad@colorado.edu

ABSTRACT

Small satellites have become capable platforms for a wide range of commercial, scientific and defense missions. Improved onboard clocks would make small satellites a viable option for even more missions, enabling radio aperture interferometry, improved radio occultation measurements, high altitude GPS navigation, and GPS augmentation missions, among others.

Previous research by the authors investigated methods for creating a high stability reference clock for small satellites by combining a heterogeneous group of oscillators including multiple CSACs, a GPS receiver and an EMXO. This work predicted that time error standard deviations of ~500 ps were possible with GPS timing errors modeled as AWGN.

This paper builds on previous work by developing a high-fidelity model for the GPS receiver timing error onboard a LEO spacecraft. Signal-In-Space Ranging Errors (SISRE) are modeled using post-fit GPS orbit and clock data, and ionospheric delays are approximated using IONEX maps and ionosphere models.

GPS point solutions are then calculated over several days of LEO orbits to generate realistic receiver timing errors, which were then used in simulations of the high-stability heterogeneous clock ensemble. Simulations show degraded clock system performance compared to the prior model, with standard deviations of time errors increasing to 1.3 ns 1-σ. The results provide insight into the nature of GPS receiver clock errors for LEOs, as well as practical limitations that should be expected when implementing advanced clock systems on small satellites.

INTRODUCTION

Accurate frequency references and timescales are increasingly important for small satellites. With low SWAP and low launch cost, smallsats are appealing for a variety of earth science and defense missions. Advancements in sensors and communication hardware have enabled smallsats to produce imagery and other data which rival much larger spacecraft [1] [1] [2] [3] [4] [5] [6] [7] [8] [9]. Cubesats have even been sent on deep space missions for the first time [10] [11].

For small satellites to serve in even more important roles, they must meet more challenging system requirements. Timekeeping is a critical area for many small satellite missions, in part because accurate position measurement requires timing accuracy. Examples of missions which require high performance timekeeping are deep space missions using one-way ranging [12], small satellite constellations functioning as sensor arrays for astronomy, and GPS augmentation missions [13].

Recently, Chip Scale Atomic Clocks (CSACs) for space were introduced [14] [15]. These devices provide very good stability for timeframes of a few hours, with very low power ($1/8^{th}$ of a Watt) and a small form-factor, and they are relatively inexpensive (< $10k). However, CSACs alone do not provide enough long-term stability for some missions without external synchronization. CSACs also have relatively poor stability for timeframes less than 100 seconds, and much higher phase noise than less expensive crystal oscillators. By combining CSACs with other clocks, both short term and long-term stability can be improved.

Previous research by the authors investigated methods for creating a high stability reference clock for small satellites by combining a heterogeneous group of

oscillators including multiple CSACs, a GPS receiver and an Evacuated Miniature Crystal Oscillator (EMXO). Two methods for combining clocks were studied: Phase Locked Loops (PLLs), and Kalman filters. The performance of the two methods was compared for LEO missions with and without a GPS reference. This work demonstrated that RMS time errors of ~500 ps would be possible with GPS timing errors modeled as additive white Gaussian noise.

This paper builds on that previous work by developing a high-fidelity model for the GPS timing error onboard a LEO spacecraft. Signal-In-Space Ranging Errors (SISRE) are computed using precise post-fit GPS orbit and clock data, along with broadcast ephemerides and clock corrections. Ionospheric delays are simulated based on IONEX maps, for typical and worst-case conditions, and corrections based on broadcast ionospheric parameters are applied for some scenarios. Finally, SISRE and ionospheric errors are incorporated into simulated pseudoranges, and point solutions are calculated over periods of several days. Realistic timing errors from the LEO point solution simulations are then used in simulations of the high-stability heterogeneous clock ensemble.

HETEROGENEOUS CLOCK SYSTEM SIMULATIONS

Previous work focused on combining CSACs with an EMXO and a GPS time reference, as show in Figure 1. The relative offsets of each of the four CSACs from the EMXO are measured, and the CSAC-EMXO offsets are averaged. The offset of the GPS time from the EMXO is also measured, and the $CSAC_{avg}$-EMXO value is subtracted from the GPS-EMXO offset, to produce the GPS-$CSAC_{avg}$ offset.

In both cases, the time offset measurement is performed using a high rate processing clock in the FPGA (300 MHz or 1 GHz). Counters operating at this higher clock frequency measure the relative delay of digital 1 PPS or 10 MHz signals from the CSACs and GPS receiver, to provide CSAC-EMXO and GPS-EMXO time offset measurements. Recall that the resolution for the 300 MHz counter is 3.3 ns, and the resolution for the 1 GHz counter is 1 ns.

Either a Kalman filter or a PLL is used estimate the low frequency (long term) error of the $CSAC_{avg}$ from the GPS-$CSAC_{avg}$. Each of these methods is described in detail in the following sections. The PLL has a narrow bandwidth (10 or 20 mHz double sided), and the Kalman filter has a high measurement noise parameter, so that both significantly attenuate the broadband GPS timing errors. The estimators also ignore the short-term fluctuations of the $CSAC_{avg}$, providing only the long-term errors. The estimated long-term error of the $CSAC_{avg}$ is subtracted from the $CSAC_{avg}$-EMXO value, and the result is passed to the loop filter for the EMXO disciplining PLL.

The EMXO PLL loop filter generates an estimate of the frequency error of the EMXO. This value is converted to an analog voltage using a low speed serial DAC, and used to adjust the frequency of the EMXO to minimize time error.

Figure 2 shows the expected effect of the low frequency error estimation and removal on the CSAC Allan deviation. CSAC errors are drastically reduced for time intervals longer than 100 seconds (which represent the low frequency components of the error), since the low frequency estimator greatly reduces the noise on the GPS time reference, enabling accurate estimation of the long-term walk of the CSAC. It is important to remember that the improved CSAC is "virtual", since it is represented as sampled differences inside the FPGA, and that the CSAC devices themselves are not being steered by the GPS reference.

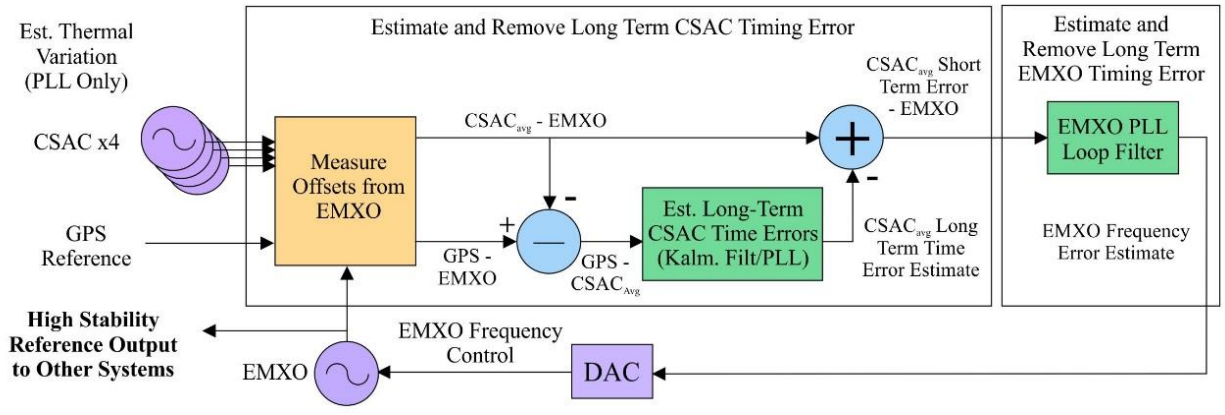

Figure 1. Block Diagram of Heterogeneous Clock System

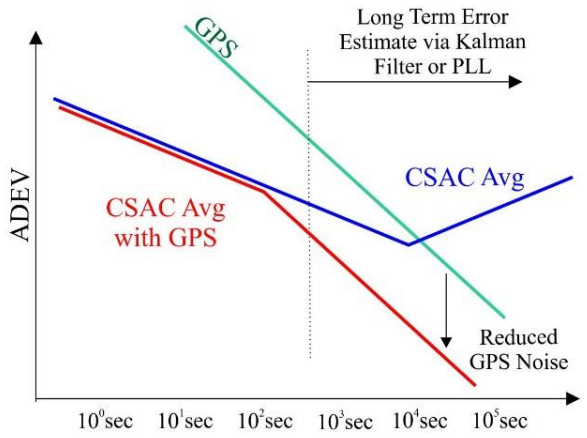

Figure 2. ADEVs for CSAC GPS Disciplining

AWGN GPS Time Error Model

The stability of GPS is often reported as having a -1:1 slope in ADEV plots, indicating that it is a White Phase Modulation (WPM) process [16]. For previous work, the GPS receiver time error was modeled as Additive White Gaussian Noise (AWGN), with a standard deviation of 10 ns. ADEVs for the EMXO, CSACs, and GPS are shown in Figure 3. Note the -1:1 slope for the GPS ADEV when modeled as AWGN.

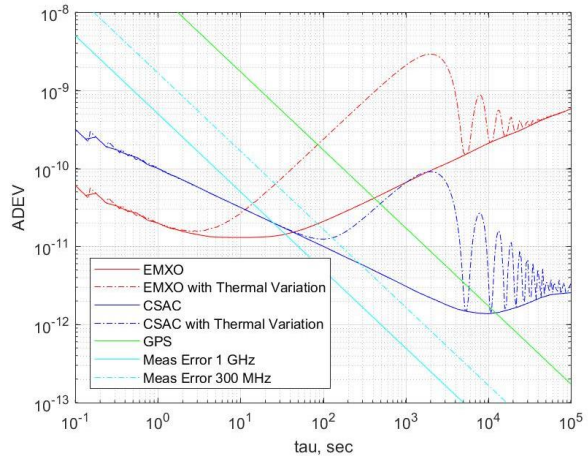

Figure 3. GPS, CSAC, and EMXO ADEVs

Using AWGN to model GPS receiver time errors was perhaps optimistic in a few ways. First, it allowed the GPS time error to be treated as measurement noise in the Kalman filtering approach for combining the CSAC and GPS time errors. It also caused the spectrum of the GPS timing errors to be broadband, making it an easy target for the low-pass behaviors of the Kalman filter and PLLs.

The performance of the GPS-CSAC combining algorithms with the AWGN GPS model is shown in Figure 4. Notice that the ADEV of the combined clock is much improved vs. the input GPS clock. For example, at 10^4 seconds, the combined ADEV has dropped from a little over 10^{-12} down to 10^{-13}, a tenfold improvement over the GPS AWGN model, and a 6x improvement over the $CSAC_{avg}$. Typical behavior for clock ensembles would limit the stability to the performance of the most stable ensemble member, in this case the $CSAC_{avg}$, with little improvement gained by combining the $CSAC_{avg}$ with GPS in this case. This overly optimistic performance assessment resulted in a standard deviation of the timing error for the EMXO-CSAC-GPS system of approximately 0.5 nanosecond.

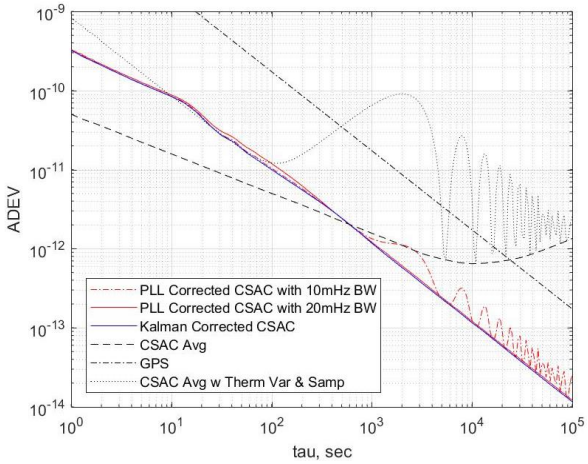

Figure 4. ADEVs for PLL and Kalman Corrected CSACs

HIGH-FIDELITY LEO GPS TIME ERROR SIMULATION

The overarching goal of this research is to characterize the achievable timing performance for LEO spacecraft. While the previous result was exciting, it had limited relevance, because it was achieved without accurately representing the characteristics of GPS receiver timing errors.

To generate representative point solution time error data for LEO spacecraft under a variety of scenarios, a more realistic simulation was developed. LEO orbit positions were calculated for several days for a circular orbit, and GPS pseudoranges including errors were used to compute point solution estimates of position and time. Point solution errors were then calculated by comparing the estimates with the true LEO position.

GPS pseudorange errors for LEO spacecraft mainly originate from the following error sources:

- Receiver Noise

- Control Segment Errors
- Ionospheric delay

Tropospheric delay is negligible for LEO altitudes, and so was also not included in the simulations.

Receiver Noise

Measurement errors on the receiver may be caused by noise or multipath. For the purposes of this study, multipath was ignored, and it was assumed that the LEO GPS antenna was selected to minimize multipath for GPS satellite above the minimum elevation of 10 degrees.

Simulated receiver noise was modeled as AWGN with a standard deviation of 5 cm [17] for single frequency scenarios, and 7.5 cm for dual frequency scenarios, to account for the added noise caused by algorithms which estimate the ionospheric delay. These noise levels assume carrier aided code tracking has been used to reduce the pseudorange noise.

Control Segment Errors

Control segment errors, also called Signal-In-Space Ranging Errors (SISRE), are errors in the broadcast orbits and clock offsets for the GPS satellites. Total SISRE values (clock + position) average approximately 0.7 m RMS across all satellites, with the clock performance varying significantly for different SVNs [18].

For this study, post-processed precise ephemerides for the Antenna Phase Center (APC) from the National Geospatial-Intelligence Agency were used for the true positions on the GPS satellites [19]. Broadcast ephemerides were also downloaded from the NGA website, and used in the computation of point solutions. Use of APC data enabled direct comparison of broadcast GPS ephemerides with the NGA data.

Because the NGA data are provided at 5-minute intervals, it was necessary to interpolate them to the 1 second sample rate. An 8-tap Lagrange interpolator was used to upsample the data. Linear interpolation was used to upsample the NGA clock estimates. Broadcast orbit elements were processed to generate the expected position and time for the GPS satellites.

Ionosphere

To model the ionosphere, Total Electron Content (TEC) maps were downloaded from the International GNSS Service (IGS) [20]. These maps provide estimates of the TEC at two-hour intervals, with 5-degree resolution in latitude and longitude.

Time interpolation was performed to estimate the TEC at times between the map epochs. Since the peak of the ionospheric activity tends to remain near 2 PM relative to the solar zenith, the map from the epoch following the desired time was rotated 30 degrees to the east, to align the peak of the ionosphere with the preceding map. Next, linear interpolation between the preceding and

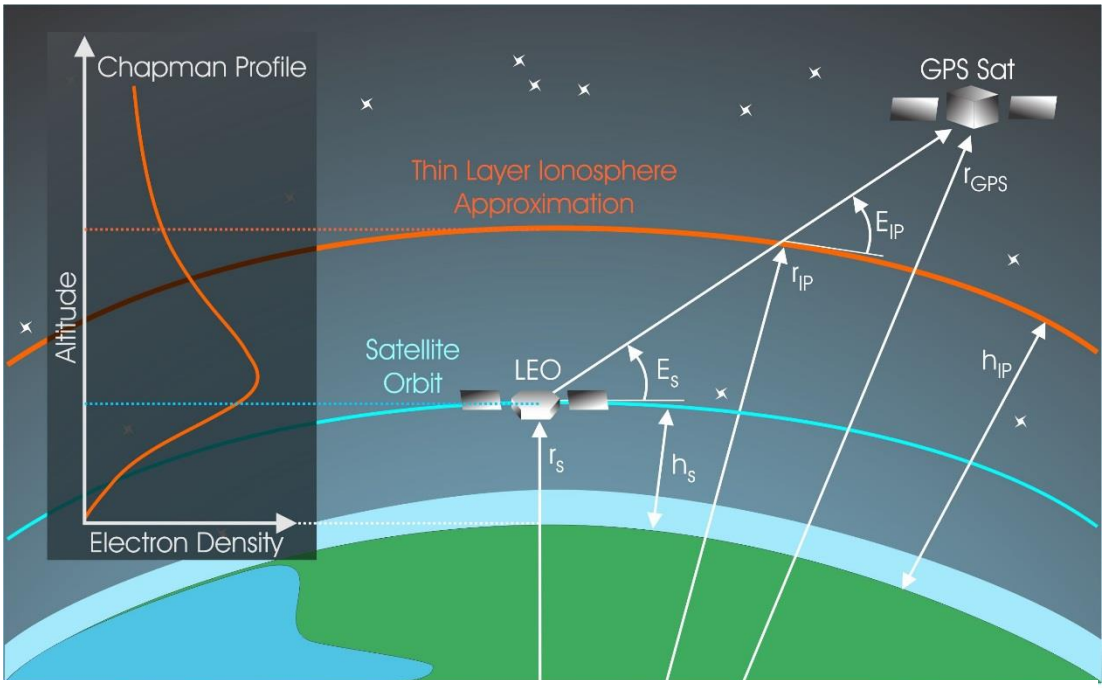

Figure 5. TEC Calculation Methodology

following maps was used to estimate the TEC map for the current time. Finally, the interpolated map was rotated back to the west to account for the earth's rotation in the interlude between the first map's epoch and the current time.

Because the TEC values given by the IGS ionex files include all the ionosphere from the ground up, the TEC remaining above the spacecraft must be estimated. We followed the methodology detailed by Montenbruck and others [21], which uses a Chapman profile (1) to estimate the fraction of the ionosphere remaining above the LEO satellite altitude. An inflection point height h_0 of 420 km and a scale height H of 100 km were used for the Chapman profile, where h is the height of the density being calculated.

$$d_e(h) = d_0 \cdot exp(1 - z - exp(-z)),\ z = (h - h_0)/H \quad (1)$$

If the effective height of the residual ionosphere h_s is defined as the altitude at which 50% of the TEC above the satellite remains, then:

$$exp(1 - exp(-z_{IP})) = \frac{1}{2}(e + exp(1 - exp(-z_S))) \quad (2)$$

where z_s is computed using the satellite height, and z_{IP} is the ionospheric pierce point height we desire.

The fraction of the TEC remaining above the satellite, α, may be computed by finding the ratio of the TEC above the satellite altitude to the total TEC:

$$\alpha = \frac{e - exp(1 - exp(-z_S))}{e - exp(1 - exp(h_0/H))} \quad (3)$$

The ionosphere is then modeled as a thin layer at the altitude which represents the midpoint of the remaining TEC above the LEO.

After calculating the thin layer height, the IPP for each GPS satellite was computed using the vectors from the LEO spacecraft position to the visible GPS satellite positions. TEC values for the IPP were estimated by interpolating the TEC map for the current time spatially with an 8-tap Lagrange filter [22].

Next, the TEC values for each of the GPS satellites were modified by an obliquity factor, which increases the TEC for GPS satellites with low elevation, to account for the longer path length.

$$\frac{1}{\sin(E_{IP})} = \left\{1 - \left[\cos(E_s) \cdot {r_s}/{r_{IP}}\right]^2\right\}^{-1/2} \quad (4)$$

Pseudorange measurements for L1 signals then experience a group delay (in seconds) of:

$$\Delta\rho_{L1} = \frac{\alpha}{\sin(E_{IP})} \frac{40.3 m^3 s^{-2}}{c f_{L1}^2} TEC(r_{IP}) \quad (5)$$

Where $TEC(r_{IP})$ is the thin layer approximation of the TEC at the radius of the IPP which was previously calculated.

When using the broadcast ionosphere model or the CODE ionosphere model to offset the ionospheric delay, the same process was used to adjust the model TEC at the IPP, given the LEO satellite altitude and obliquity.

SIMULATION SCENARIOS

The simulation scenarios demonstrate a range of different conditions, to understand the impact that the level of the ionosphere and the type of ionospheric compensation (if any) had on the time estimation performance of the LEO GPS receiver. Simulations are summarized in Table 1.

Most of the simulations were performed with a LEO altitude of 450 km, but a single simulation was run with an altitude of 1000 km to observe the effect of the greatly reduced TEC above that height. Orbits were roughly aligned so that the Right Ascension of the Ascending Node (RAAN) coincided with the 2 PM peak of the ionosphere.

A "worst case" simulation was performed using the ionospheric maps from July 29-30 of 2003, when the TEC reached a maximum of 220 TECU near the equator. The rest of the simulations used the ionospheric maps from November 24-25 of 2018.

Two of the simulations used either the broadcast TEC parameters or the Center for Orbit Determination in Europe (CODE) TEC parameters to estimate and compensate for some of the ionospheric delay [23].

Table 1. Simulation Scenarios

Simulation Name	LEO Altitude	GPS Days	Dual Frequency (Iono Free)	Iono Conditions	Iono Map Days	Iono Model
450km Worst Iono Oct. 2003	450	Nov. 24-25, 2018	No	Worst Case	Oct. 29-30, 2003	None
450km Nominal Iono	450	Nov. 24-25, 2018	No	Average	Nov. 24-25, 2018	None
450km Nom. Iono Broadcast Comp	450	Nov. 24-25, 2018	No	Average	Nov. 24-25, 2018	Broadcast
450km Nom. Iono CODE Comp	450	Nov. 24-25, 2018	No	Average	Nov. 24-25, 2018	CODE
1000km Nominal Iono	1000	Nov. 24-25, 2018	No	Average	Nov. 24-25, 2018	None
450km Iono Free	450	Nov. 24-25, 2018	Yes	N/A	N/A	N/A

All the simulations included the effects of SISRE. The data used to generate the SISRE models were from November 24-25, 2018 data for all simulations.

Receiver Time Error Simulation Results

Figure 6 shows the GPS receiver time error caused by SISRE for a 450km LEO orbit without the effect of the ionosphere (iono-free). The standard deviation of the error is 1.8 ns, and the maximum offset is over 9ns for this two-day period.

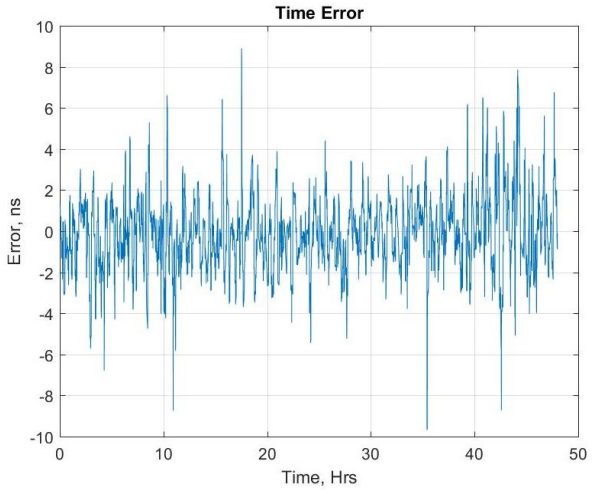

Figure 6. LEO GPS Time Error Due to SISRE for Nominal Orbit

Figure 7 shows a portion of the time error, which shows that the SISRE-induced errors are characterized by sharp jumps, connected by sloped segments. The jumps occur because the LEO spacecraft is constantly acquiring and dropping GPS satellites during its orbit, depending on which GPS satellites are visible. Because each GPS satellite has unique SISRE, the point solution adjusts to a different optimal value when satellites are added or removed. Updates to the broadcast ephemerides also cause jumps, but these typically only occur at two-hour intervals for the legacy navigation message, seen at hours 10 and 12 in this plot.

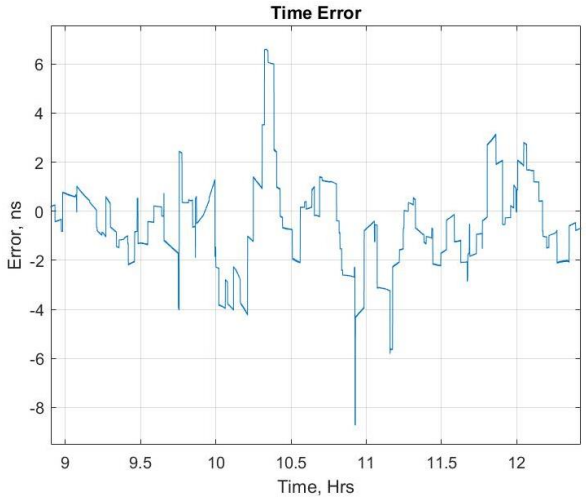

Figure 7. Zoom of 450 km SISRE Time Error

Figure 8 shows the time errors for all scenarios over one day. The worst-case ionosphere simulation shows time errors of 240 ns, worst case. Clearly, the ionosphere has the potential to significantly degrade the accuracy of the time estimate for LEO GPS receivers.

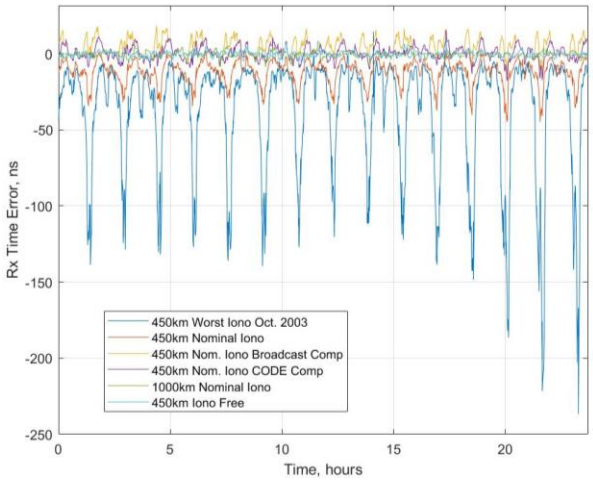

Figure 8. GPS Receiver PS Time Errors

Figure 9 shows the total non-worst-case errors over a few hours. Even the "nominal" ionosphere introduces time errors of over 40 ns. Both the broadcast model and the CODE model do a good job of removing the bias and reduce the peak errors to approximately +/- 15 ns for this brief example.

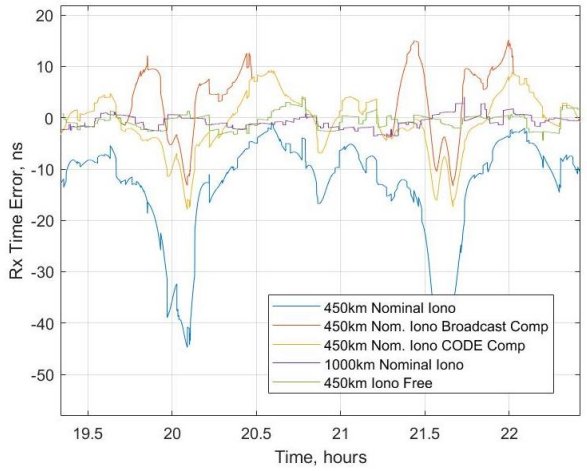

Figure 9. Zoomed PS Time Errors Without Worst Case

GPS POINT SOLUTION TIME STABILITY

Figure 10 shows the Allan deviations for all scenarios. The effect of the ionosphere is evident here as well, with the "nominal ionosphere" case nearly 5x less stable for timeframes from 1,000 seconds to 100,000 seconds. The worst-case ionosphere results in 20x reduction in stability. Here the benefit of using ionospheric models is evident, with the CODE model providing a nearly 2x improvement over the uncompensated nominal ionosphere, and the broadcast model only slightly worse.

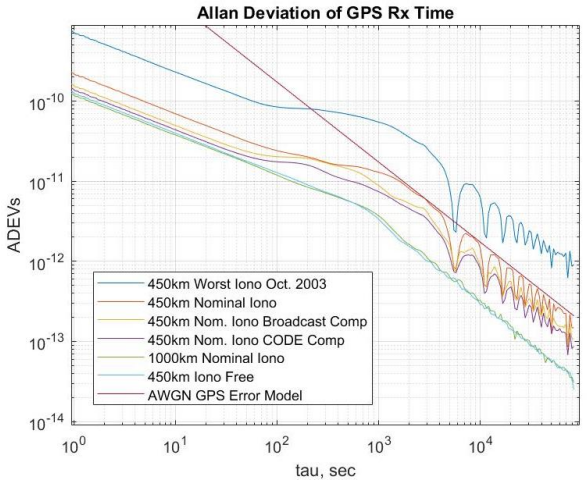

Figure 10. Allan Deviations for All Scenarios

Some cause for using AWGN with a 10 ns standard deviation is also evident: the AWGN matches the peaks of the receiver time stability with nominal, uncompensated ionosphere well for timeframes above 1,000 seconds. However, the AWGN model with 10 ns standard deviation appears overly pessimistic for the iono-free or 1000 km scenarios, which have ADEVs approximately 6x lower.

Table 2 shows the time error standard deviations and biases for the different scenarios, ordered from worst to best. For the 450 km orbit, the GPS receiver reference time output will clearly be compromised by the ionosphere, even with compensation, indicating that a dual frequency, iono-free approach is best for missions with lower LEO orbits and tight timing requirements. The 1000 km orbit experiences much smaller ionospheric effects, even with no compensation and a single frequency GPS receiver.

Table 2. GPS Rx Time Error Standard Deviations and Biases

Simulation Name	Time Error Standard Deviation, ns	Time Error Bias, ns
450km Worst Iono Oct. 2003	35.2	-32.8
450km Nominal Iono	7.9	-11.8
450km Nom. Iono Broadcast Comp	5.4	4.3
450km Nom. Iono CODE Comp	4.6	0.7
1000km Nominal Iono	1.9	-0.2
450km Iono Free	1.8	-0.1

CLOCK ENSEMBLE SIMULATION

The goal of the GPS receiver simulations was to create high fidelity models of the receiver time error, to then use in LEO high-stability clock system simulations. But before discussing the high-stability clock system performance, it is important to understand another key impairment in the system: thermal errors in the CSAC and EMXO clocks.

Thermal Errors

Because small satellites have extremely low operating power, sometimes less than 15 Watts, they do not actively manage the temperature of onboard electronics. As a result, the temperature onboard a small satellite in a LEO orbit may fluctuate by as much as 40 degrees C. Although clocks such as the EMXO and CSAC are designed to minimize frequency errors caused by temperature variations, this large temperature fluctuation is enough to induce significant time variations over a 100 minute LEO orbit [24].

The EMXO datasheet lists the frequency sensitivity of the device to temperature as 10 ppb over a 50 degree range. The CSAC datasheet lists its frequency sensitivity as 0.5 ppb for an 80 degree C range. These sensitivities result in significant time errors over each orbit, as shown in Figure 11, for a 40 degree sinusoidal variation in temperature and a linear relationship between temperature and frequency error. Note that the thermally induced time variations are significant compared to the values of the random walk over a few days.

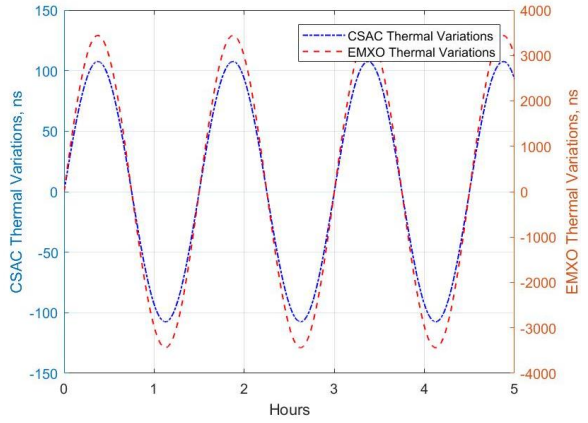

Figure 11. CSAC and EMXO Time Errors Due to Temperature Change

The impact of the thermal frequency error is also apparent in the CSAC and EMXO Allan deviation plots of Figure 3. Stability for averaging times longer than 10 seconds is severely degraded. Clearly, the thermal variations must be estimated and removed to achieve high system time stability.

Correlation in Ionospheric and Thermally Induced Time Errors

For single frequency GPS receivers, the time error induced by ionospheric delay occurs due to changes in the ionosphere over the orbit, as the LEO spacecraft passes close to the 2PM mark near the solar zenith. This gives the ionospheric delay a fundamental period equal to the orbital period. Similarly, the CSAC and EMXO timing errors caused by thermal variation also occur due to temperature changes over the orbit of the LEO spacecraft. Because the two errors share the same fundamental period (1 orbit), it is much more difficult to separate thermal variation in the CSAC and EMXO from ionospheric variation in the GPS receiver.

For this reason, no attempt was made to simulate a system which has both thermal variations in the CSACs and EMXOs, and ionospheric variations in the GPS receiver.

Kalman Filtering Approach for Estimating CSAC Errors

GPS receiver time error was treated as measurement error during simulations which used a Kalman filter to estimate and remove CSAC variations. Even if the ionospheric impairments are removed, the GPS receiver time error caused by SISRE is not AWGN, so without simulation, it is unclear whether it makes sense to treat the GPS time error as measurement error in the Kalman filter.

The CSAC was modeled using White FM (WFM) and Random Walk FM (RWFM) elements of the power law model [25]. For a clock with WFM and RWFM, the clock state propagates according to the following equations, with τ representing the sample period:

$$\boldsymbol{x_{k+1} = x_k + \tau y_k + \varepsilon_k, \varepsilon_k \sim N(0, \sigma_{WFM})} \quad \textbf{(6)}$$

$$\boldsymbol{y_{k+1} = y_k + \eta_k, \eta_k \sim N(0, \sigma_{RWFM})} \quad \textbf{(7)}$$

where x represents the clock phase and y represents the clock frequency. The values ε and η represent the noise in the clock states. The corresponding state propagation matrix is:

$$\boldsymbol{\Phi} = \begin{pmatrix} \mathbf{1} & \boldsymbol{\tau} \\ \mathbf{0} & \mathbf{1} \end{pmatrix} \quad \textbf{(8)}$$

The process covariance matrix Q is given by:

$$\mathbf{Q} = \begin{pmatrix} \left[\boldsymbol{\sigma_{WFM}^2 \tau + \frac{\sigma_{RWFM}^2 \tau^3}{3}}\right] & \left[\boldsymbol{\frac{\sigma_{RWFM}^2 \tau^2}{2}}\right] \\ \left[\boldsymbol{\frac{\sigma_{RWFM}^2 \tau^2}{2}}\right] & \left[\boldsymbol{\sigma_{RWFM}^2 \tau}\right] \end{pmatrix} \quad \textbf{(9)}$$

Implementing the approach introduced by Rybak, et al. [24], a second order Gauss Markov process was used for the sinusoidal thermal frequency variations. This technique is called Dynamic Model Compensation (DMC). For a clock with WFM, RWFM, and a purely oscillatory thermal model, the full state propagation matrix is:

$$\boldsymbol{\Phi} = \begin{pmatrix} \mathbf{1} & \boldsymbol{\tau} & \mathbf{0} & \mathbf{0} \\ \mathbf{0} & \mathbf{1} & \boldsymbol{\tau} & \mathbf{0} \\ \mathbf{0} & \mathbf{0} & \boldsymbol{cos(\omega\tau)} & \boldsymbol{\frac{1}{\omega} sin(\omega\tau)} \\ \mathbf{0} & \mathbf{0} & \boldsymbol{-\omega sin(\omega\tau)} & \boldsymbol{cos(\omega\tau)} \end{pmatrix} \quad \textbf{(10)}$$

And the process noise matrix of the DMC is given by:

$$\mathbf{Q} = \boldsymbol{\sigma^2} \begin{pmatrix} \boldsymbol{a^2} & \mathbf{ab} \\ \mathbf{ba} & \boldsymbol{b^2} \end{pmatrix} \quad \textbf{(11)}$$

Where

$$\boldsymbol{a = \sqrt{2\sigma^2 \omega}} \quad \textbf{(12)}$$

$$\boldsymbol{b = \sqrt{2\sigma^3 \omega^3}} \quad \textbf{(13)}$$

Clock Ensemble Formation

For systems with no thermal time error on CSAC and EMXO clocks, it is possible to use a Kalman clock ensemble to combine the GPS receiver and $CSAC_{avg}$ times. This would differ from the approach previously used, in that the GPS time error would be included in the Kalman states. Because of the periodic nature of the ionosphere induced time error, a 2nd order Gauss Markov process would be included in the GPS states, rather than the CSAC states. The Basic Time-Scale Equation

(BTSE) would be used to assign differences in time between CSAC and GPS to the most likely states [26].

However, because the $CSAC_{avg}$ time stability is not significantly better than the GPS time stability with ionospheric impairments, little gain is anticipated from forming an ensemble from the two. For this reason, only iono-free GPS time estimates were used in the EMXO-CSAC-GPS system stability simulations.

EMXO-CSAC-GPS CLOCK FORMATION

To characterize the achievable performance for a LEO EMXO-CSAC-GPS clock, the 450 km iono-free GPS receiver time errors were used in the time system simulation. Simulations were performed with thermal variations in the CSACs and EMXO.

Figure 12 shows the ADEV for the system which uses the Kalman filter to combine GPS and CSAC times, and a PLL to combine the corrected CSAC time with the EMXO time. The system clock shows stability improvement vs. GPS, $CSAC_{avg}$, and the EMXO for most tau values. The standard deviation for the resulting high-fidelity clock is 1.3 ns, a significant improvement over the GPS time error, which was 1.8 ns. By using the 2nd order Gauss Markov process for DMC, the thermal variation of the CSAC and EMXOs has been mitigated.

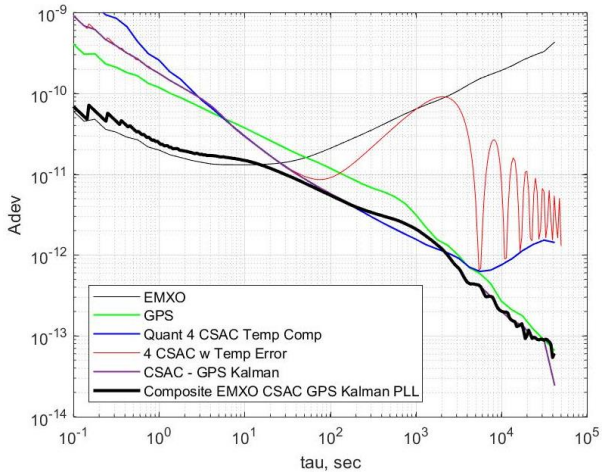

Figure 12. High-Stability Clock System with Iono-Free GPS and CSAC/EMXO Thermal Impairment

Figure 13 compares the performance of the EMXO-CSAC-GPS clock system with the 450 km LEO SISRE errors against the system with the AWGN GPS model. Although the stability of the AWGN GPS clock model is much worse than the 450 km LEO SISRE simulation across all time frames, the Kalman filter effectively combines the AWGN GPS error with the CSAC and EMXO, leading to a lower total system error. The non-AWGN character of the simulated GPS with SISRE errors prevents the Kalman filter from improving the overall stability for time frames above 1000 seconds.

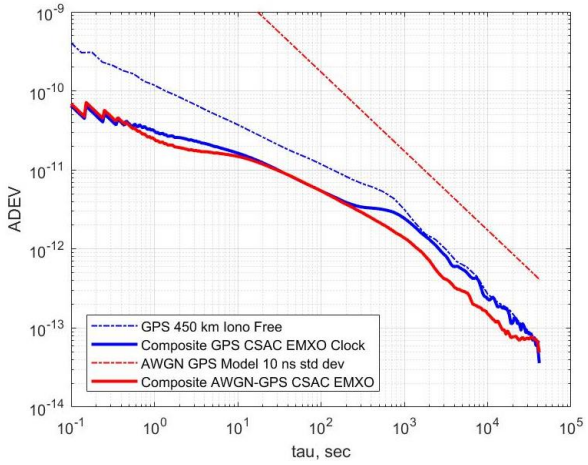

Figure 13. Clock Performance with LEO GPS SISRE Error Model vs AWGN

CONCLUSIONS

Simulation of the time estimates for a LEO GPS receiver revealed two key pieces of information:

- The ionosphere significantly reduces the receiver time stability unless a) a dual frequency receiver is used to estimate and remove the ionospheric delays, or b) the LEO orbit is high enough to eliminate most of the ionospheric delay.
- If the ionospheric delay is reduced or eliminated, the remaining time error, dominated by SISRE, is not AWGN below 1000 seconds.

Plugging the simulated receiver time error from the 450 km iono-free scenario into the high-fidelity clock system simulations developed earlier showed that the system clock performance was better than the GPS receiver time estimate alone (1.3 ns vs. 1.8 ns), and that the thermal errors of the CSAC and EMXO clocks could be mitigated. It also showed that the time system error, which was previously 0.5 ns when modeling GPS as a 10 ns standard deviation AWGN signal, was overly optimistic.

REFERENCES

[1] W. Williams, C. Coen, M. Frounchi, N. Lourenco and J. D. Cressl, "Micronimbus: A cubesat temperature profilometer for the earth's atmosphere using a single-chip 60 GHZ sige radiometer," in *IEEE International*

Geoscience and Remote Sensing Symposium (IGRSS), Fort Worth, 2017.

[2] G. Chattopadhyay, "Terahertz Instruments for CubeSats," in *IEEE MTT-S International Microwave and RF Conference (IMaRC)*, Ahmedabad, 2017.

[3] S. A. Ali Shah and U. Arshad, "General system design of Cubesat in LEO for IR imaging," in *International Conference on Aerospace Science & Engineering (ICASE)*, Islamabad, 2013.

[4] C. D. Norton, P. S. Millar, R. Bauer and G. J. Komar, "New capabilities for Earth Science measurements with 6U CubeSat technologies," in *IEEE International Geoscience and Remote Sensing Symposium (IGARSS)*, Beijing, 2016.

[5] C. J. Galbraith, "An LTCC-based 8-channel 4 to 12 GHz hybrid channel-dropping multiplexer for a CubeSat radiometer mission," in *IEEE MTT-S International Microwave Symposium (IMS)*, Honololu, 2017.

[6] E. Peral, S. Tanelli, Z. Haddad, O. Sy, G. Stephens and E. Im, "Raincube: A proposed constellation of precipitation profiling radars in CubeSat,," in *2015 IEEE International Geoscience and Remote Sensing Symposium (IGARSS)*, Milan, 2015.

[7] E. Kalemci, E. Ümit and R. Aslan, "X-ray detector on 2U cubesat BeEagleSAT of QB50," in *2013 6th International Conference on Recent Advances in Space Technologies (RAST)*, Istanbul, 2013 .

[8] E. W. Bryerton, J. L. Hesler, S. A. Retzloff and T. W. Crowe, "874-GHz heterodyne CubeSat receiver for cloud ice measurements - flight model data," in *2016 IEEE International Geoscience and Remote Sensing Symposium (IGARSS)*, Beijing, 2016 .

[9] L. Alminde and K. K. Laursen, "A strategic approach to developing space capabilities using Cubesat technology," in *2009 4th International Conference on Recent Advances in Space Technologies*, Istanbul, 2009 .

[10] R. E. Hodges, N. Chahat, D. J. Hoppe and J. D. Vacchione, "A Deployable High-Gain Antenna Bound for Mars: Developing a new folded-panel reflectarray for the first CubeSat mission to Mars," *IEEE Antennas and Propagation Magazine*, pp. 39-49, April 2017.

[11] B. Segret, D. Hestroffer, G. Quinsac, M. Agnan, J. Vannitsen and B. Mosser, "In-flight orbit determination for a deep space CubeSat," in *2018 IEEE Aerospace Conference*, Big Sky, MT, 2018 .

[12] T. Imken, J. Castillo-Rogez, Y. He, J. Baker and A. Marinan, "CubeSat flight system development for enabling deep space science," in *2017 IEEE Aerospace Conference*, Big Sky, MT, 2017 .

[13] T. G. Reid, A. M. Neish, T. F. Walter and P. K. Enge, "Leveraging Commercial Broadband LEO Constellations for Navigating," in *Proceedings of the 29th International Technical Meeting of The Satellite Division of the Institute of Navigation (ION GNSS+ 2016)*, Portland, Oregon, 2016.

[14] Microsemi, "Quantum SA.45s CSAC, Chip Scale Atomic Clock Datasheet," Microsemi.

[15] P. Cash, "Microsemi Chip Scale Atomic Clock (CSAC) technical status, applications, and future plans," in *European Frequency and Time Forum (EFTF)*, Turin, 2018.

[16] V. Ogrizovic, J. Marendic, S. Renovica, S. Del and J. Gucevic, "Testing GPS generated 1PPS against a rubidium standard," *ACTA IMEKO*, vol. 2, no. 1, 2013.

[17] P. Misra and P. Enge, Global Positioning System: Signals, Measurement, and Performance, Lincoln, Massachusetts, USA: Ganga-Jamuna Press, 2001.

[18] O. Montenbruck, P. Steigenberger and A. Hauschild, "Broadcast versus precise ephemerides: a multi-GNSS perspective," *GPS Solutions*, vol. 19, pp. 321-333, 2015.

[19] NGA, "NGA Office of Geomatics," 2019. [Online]. Available: http://earth-info.nga.mil. [Accessed April 2019].

[20] IGS, "GNSS Ionosphere Products," International GNSS Service, 2019. [Online]. Available: ftp://cddis.gsfc.nasa.gov/gnss/products/ionosphere/. [Accessed 2019].

[21] O. Montenbruck and E. Gill, "Ionospheric Correction for GPS Tracking of LEO Satellites," *The Journal of Navigation*, pp. 293-304, 2002.

[22] T. Laakso, V. Valimaki, M. Karjalainen and U. Laine, "Splitting the Unit Delay," *IEEE Signal Processing Magazine*, pp. 30-60, January 1996.

[23] CODE, "CODE Ionosphere Parameter Download FTP Site," CODE, 2019. [Online]. Available: http://ftp.aiub.unibe.ch/CODE. [Accessed 2019].

[24] M. Rybak, P. Axelrad and J. Seubert, "Investigation of CSAC Driven One-Way Ranging Performance for CubeSat Navigation," in *32nd Annual AIAA/USU Conference on Small Satellite*, 2018.

[25] L. Galleani, "A tutorial on the two-state model of the atomic clock noise," *Metrologia*, 2008.

[26] S. R. Stein, "Time scales demystified," in *IEEE International Frequency Control Symposium and PDA Exhibition Jointly with the 17th European Frequency and Time Forum*, Tampa, FL, 2003.

[27] R. Fields, X. Sun, J. B. Abshire, J. Beck, R. M. Rawlings, W. Sullivan III and D. Hinkley, "A linear mode photon-counting (LMPC) detector array in a CubeSat to enable earth science LiDAR measurements," in *IEEE International Geoscience and Remote Sensing Symposium (IGARSS)*, Milan, 2015.